PHYSICAL REVIEW D **89,** 061303(R) (2014)

Impact of active-sterile neutrino mixing on supernova explosion and nucleosynthesis

Meng-Ru Wu,[1] Tobias Fischer,[2] Lutz Huther,[1] Gabriel Martínez-Pinedo,[1,3] and Yong-Zhong Qian[4]

[1]*Institut für Kernphysik (Theoriezentrum), Technische Universität Darmstadt, Schlossgartenstraße 2, 64289 Darmstadt, Germany*

[2]*Institute for Theoretical Physics, University of Wrocław, Plac Maksa Borna 9, 50-204 Wrocław, Poland*

[3]*GSI Helmholtzzentrum für Schwerioneneforschung, Planckstraße 1, 64291 Darmstadt, Germany*

[4]*School of Physics and Astronomy, University of Minnesota, Minneapolis, Minnesota 55455, USA*

(Received 10 May 2013; revised manuscript received 15 November 2013; published 17 March 2014)

We show that for the active-sterile flavor mixing parameters suggested by the reactor neutrino anomaly, substantial ν_e-ν_s and $\bar{\nu}_e$-$\bar{\nu}_s$ conversion occurs in regions with an electron fraction of $\approx 1/3$ near the core of an $8.8 M_\odot$ electron-capture supernova. We explicitly include the feedback of such conversion on the evolution of the electron fraction in supernova ejecta. Compared to the case without such conversion, the neutron richness of the ejecta is enhanced to allow production of elements from Sr, Y, and Zr up to Cd in broad agreement with observations of the metal-poor star HD 122563 for a wide range of mixing parameters. Active-sterile flavor conversion can also strongly suppress neutrino heating at times when it is important for the revival of the shock. Our results suggest that simulations of a supernova explosion and the associated nucleosynthesis may be used to constrain active-sterile mixing parameters in combination with neutrino experiments and cosmological considerations.

DOI: 10.1103/PhysRevD.89.061303 PACS numbers: 97.60.Bw, 14.60.Pq, 26.30.-k

The number of active neutrino flavors that participate in weak interactions in the Standard Model has been precisely determined from the Z^0 decay width to be 2.984 ± 0.008 [1]. Nearly all the vacuum mixing parameters for active neutrinos have been measured, except for the mass hierarchy and the CP violating phase [2]. However, recent results on oscillations of neutrinos from reactors, radioactive sources, and accelerators indicate that the standard mixing scenario involving only the three active flavors may not be complete [3–7]. Light sterile neutrinos (ν_s) of the eV mass scale that mix with active neutrinos have been proposed as the simplest extension beyond the standard scenario to explain these anomalies (see [8] for a recent review). While the so-called reactor neutrino anomaly [6] may be affected by the uncertainties of the reactor neutrino spectrum [9], the Gallium anomaly [10] remains to be explained. On the other hand, the effective relativistic degree of freedom inferred from both cosmic microwave background data and big bang nucleosynthesis studies has large enough uncertainties to also allow such sterile neutrinos to exist [11–13]. There is some tension between the sterile neutrino parameters obtained from different oscillation experiments and cosmological constraints [14–16]. This will be resolved by future experiments including solar neutrino measurements [8].

In addition to important implications for experiments and cosmology, the mixing of sterile with active neutrinos may lead to multiple Mikheyev-Smirnov-Wolfenstein resonances in matter [17–21], which could have interesting effects in supernovae [21–33]. In particular, [22] pointed out that for light sterile neutrinos of 1–100 eV, ν_e-ν_s and $\bar{\nu}_e$-$\bar{\nu}_s$ conversion could have a significant impact on the supernova explosion and nucleosynthesis. As such a conversion changes the electron fraction Y_e, and hence the matter potential determining the Mikheyev-Smirnov-Wolfenstein resonances, this feedback should be included in a full treatment of the problem. Possible feedback effects were noted in [22] and taken into account in some later works (e.g., [27,28,33]), which mostly focused on the outer resonances at baryon densities of $\rho < 10^8$ g cm^{-3}.

In this paper we examine active-sterile flavor conversion (ASFC) in the region of the inner resonances (IR) where $\rho \sim 10^9$–10^{12} g cm^{-3} and evaluate its impact on supernova dynamics and nucleosynthesis with a careful treatment of its feedback on the evolution of Y_e in supernova ejecta. A supernova starts when a massive star undergoes gravitational core collapse at the end of its life. Upon reaching supranuclear density, the core bounces to launch a shock and a protoneutron star forms and cools by emitting all three flavors of active (anti)neutrinos. As the shock propagates out of the core, it loses energy by dissociating nuclei in the material falling through it into free nucleons. At the same time, the dissociated material behind the shock gains energy from neutrino heating mainly by the following reactions:

$$\nu_e + n \rightarrow p + e^-, \tag{1a}$$

$$\bar{\nu}_e + p \rightarrow n + e^+. \tag{1b}$$

This is the essence of the so-called delayed neutrino-heating explosion mechanism [34], which has been shown to result in explosions in recent supernova simulations [35–37]. Reactions (1a) and (1b) and their reverse reactions

are essential to determining the Y_e and hence, nucleosynthesis in any neutrino-heated ejecta [38–40]. ASFC of the ν_e-ν_s and $\bar{\nu}_e$-$\bar{\nu}_s$ types may influence the rates of reactions (1a) and (1b), and consequently, affect supernova dynamics and nucleosynthesis.

To treat ASFC in supernovae, we assume effective 2-ν mixing between ν_e and ν_s ($\bar{\nu}_e$ and $\bar{\nu}_s$). This is justified as the magnitude of the mass-squared difference $\delta m^2 \sim \mathcal{O}(\pm 1)$ eV^2 between the relevant vacuum mass eigenstates greatly exceeds those for mixing among active neutrinos, and collective oscillations among active neutrinos are expected to be suppressed due to the high matter density in the region of interest to us [41]. We further assume that nearly all neutrinos freely stream through this region due to their large mean-free path. Under these assumptions, a ν_e-ν_s resonance occurs when

$$\frac{\delta m^2}{2E_\nu}\cos 2\theta = \frac{3\sqrt{2}}{2} G_F n_b \left(Y_e - \frac{1}{3}\right) = V^{\rm eff}_{\nu_e}, \qquad (2)$$

where θ is the vacuum mixing angle, E_ν is the neutrino energy (with average values of $\langle E_\nu \rangle \sim 10$–$15$ MeV), G_F is the Fermi coupling constant, and $n_b = \rho/m_u$ is the baryon number density with m_u being the atomic mass unit. The right-hand side of Eq. (2) is the effective potential $V^{\rm eff}_{\nu_e}$ from ν_e forward scattering on neutrons, protons, and $e^\pm$ in matter [21,22]. Compared to $V^{\rm eff}_{\nu_e} \sim \sqrt{2} G_F n_b$ for radii r of interest, the contribution of ν-ν forward scattering [42–44] $V^{\rm eff}_{\nu\text{-}\nu} \sim 2\sqrt{2} G_F (n_{\nu_e} - n_{\bar{\nu}_e})(R_\nu/r)^2$ is 2 orders of magnitude smaller [see Fig. 1(a)], and therefore will be neglected. Here $n_{\nu_e(\bar{\nu}_e)}$ is the ν_e ($\bar{\nu}_e$) number density and R_ν is the radius of the neutrinosphere.

In supernovae, the central Y_e is $\lesssim 0.3$ after a core bounce as a result of electron capture on nuclei and free protons during core collapse [45,46]. With increasing radius, Y_e becomes as as low as 0.1 near the neutrinospheres due to electron capture on shock-dissociated material. At even larger radii, Y_e increases to ~ 0.5 due to reactions (1a) and (1b) [see Fig. 1(a)]. Consequently, above the ν_e sphere at $r = R_{\nu_e}$, there is a radius, $R_{\rm IR}$, where $Y_e = 1/3^+$ but $\sqrt{2} G_F n_b \gg \delta m^2/2E_\nu$, and Eq. (2) is satisfied for $\delta m^2 > 0$ (normal hierarchy). For typical density profiles, this IR corresponds to $\rho \sim 10^9$–10^{12} g cm^{-3}. A second outer resonance (OR) occurs further out at larger values of Y_e once n_b drops enough to satisfy Eq. (2) [see Fig. 1(b)]. The condition for a $\bar{\nu}_e$-$\bar{\nu}_s$ resonance differs from Eq. (2) by an opposite sign of the effective potential, $V^{\rm eff}_{\bar{\nu}_e} = -V^{\rm eff}_{\nu_e}$. If $\delta m^2 > 0$, an IR occurs for $\bar{\nu}_e$-$\bar{\nu}_s$ conversion for $Y_e = 1/3^-$ but there is no OR in this case. If $\delta m^2 < 0$ (inverted hierarchy), there would be only an IR for ν_e-ν_s conversion but both an IR and an OR for $\bar{\nu}_e$-$\bar{\nu}_s$ conversion.

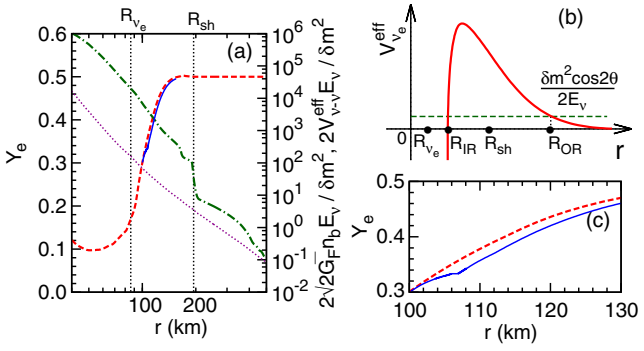

FIG. 1 (color online). (a) Profiles of Y_e with (blue solid curve) and without (red dashed curve) ASFC for $\delta m^2 = 1.75$ eV^2 and $\sin^2 2\theta = 0.10$, and of $2\sqrt{2} G_F n_b E_\nu/\delta m^2$ (green dash-dotted curve) and $2V^{\rm eff}_{\nu\text{-}\nu} E_\nu/\delta m^2$ (magenta dotted curve) for $E_\nu = 10$ MeV, at $t_{\rm pb} \sim 34$ ms. (b) Schematic plot of $V^{\rm eff}_{\nu_e}$ (red solid curve) as a function of radius, illustrating the positions of different resonances with respect to the ν_e sphere (R_{ν_e}) and the shock ($R_{\rm sh}$). (c) Blowup of the Y_e profiles in (a) for $r \gtrsim R_{\rm IR}$.

It is clear from the above discussion that independent of the mass hierarchy and for $|\delta m^2| \lesssim 10$ eV^2, there is always an IR for both ν_e-ν_s and $\bar{\nu}_e$-$\bar{\nu}_s$ conversion at $Y_e \approx 1/3$ in supernovae. [There is only an OR for ν_x-ν_s or $\bar{\nu}_x$-$\bar{\nu}_s$ ($x = \mu$, τ) conversion as $V^{\rm eff}_{\nu_x} \propto (1 - Y_e)$.] However, an inverted hierarchy appears disfavored by neutrino mass constraints from the cosmic microwave background and tritium decay experiments [47–49]. Therefore, we will not discuss this case further but will focus on the IR at $Y_e \approx 1/3$ for a normal hierarchy with $\delta m^2 > 0$ below.

As $\sqrt{2} G_F n_b \gg \delta m^2/2E_\nu$ in the region of interest, the local effective neutrino mass eigenstates are determined by $V^{\rm eff}_{\nu_e}$ except near the IR. At $r < R_{\rm IR}$ where $Y_e < 1/3$ gives $V^{\rm eff}_{\nu_e} < 0$, the lighter (heavier) effective mass eigenstate ν_L (ν_H) is approximately ν_e (ν_s), while at $r > R_{\rm IR}$ where $Y_e > 1/3$ gives $V^{\rm eff}_{\nu_e} > 0$, ν_L (ν_H) is approximately ν_s (ν_e). With $V^{\rm eff}_{\bar{\nu}_e} = -V^{\rm eff}_{\nu_e}$, the situation is exactly the opposite for the effective antineutrino mass eigenstates. As ν_e ($\bar{\nu}_e$) cross $R_{\rm IR}$ from below, the probability that they hop from ν_L ($\bar{\nu}_H$) to ν_H ($\bar{\nu}_L$) can be approximated by the Landau-Zener formula [50,51]:

$$P_{\rm hop}(E_\nu, \mu) = \exp\left(-\frac{\pi^2}{2}\frac{\delta r}{L}\right), \qquad (3)$$

where $\delta r = \delta m^2 \sin 2\theta/(\mu E_\nu |dV^{\rm eff}_{\nu_e(\bar{\nu}_e)}/dr|_{\rm res})$ is the width of the resonance region with μ the cosine of the angle between the ν_e ($\bar{\nu}_e$) momentum and the radial direction, and $L = 4\pi E_\nu/(\delta m^2 \sin 2\theta)$ is the oscillation length at resonance [52]. Taking $\delta m^2 = 1.75$ eV^2 and $\sin^2 2\theta = 0.10$, which are the best-fit parameters inferred from reactor neutrino experiments [14], we obtain $L \approx 45$ m for $E_\nu = 10$ MeV. As $|Y_e - 1/3| \ll 1$ at the IR, $|dV^{\rm eff}_{\nu_e(\bar{\nu}_e)}/dr|_{\rm res} \approx (3\sqrt{2}/2) G_F (\rho_{\rm res}/m_u) |dY_e/dr|_{\rm res}$. Using the same mixing parameters as above and taking $\rho_{\rm res} = 10^9$ g cm^{-3}, $|dY_e/dr|_{\rm res} = 10^{-2}$ km^{-1}, and $\mu = 1$, we obtain $\delta r \approx 48$ m for $E_\nu = 10$ MeV. In the above example, $\delta r \gtrsim L$ gives $P_{\rm hop} \sim 0$, which means that

ν_e ($\bar{\nu}_e$) produced originally as ν_L ($\bar{\nu}_H$) will stay in their local effective mass eigenstates, and after crossing the IR, be completely converted into ν_s ($\bar{\nu}_s$).

In general, $\delta r/L \propto (\delta m^2 \sin 2\theta/E_\nu)^2(\rho|dY_e/dr|)^{-1}_{\rm res}/\mu$ and therefore, $P_{\rm hop}(E_\nu,\mu)$ is sensitive to dY_e/dr at $Y_e \approx 1/3$. We define $E_{0.5}$ as the E_ν corresponding to $P_{\rm hop} = 0.5$ for $\mu = 1$. It is clear from Eq. (3) and the above discussion that most of the ν_e ($\bar{\nu}_e$) with $E_\nu < E_{0.5}$ will be converted into ν_s ($\bar{\nu}_s$) after passing through the IR ($P_{\rm hop} \sim 0$), while most of those with $E_\nu > E_{0.5}$ will survive in their initial flavor states ($P_{\rm hop} \sim 1$).

The sensitivity of $P_{\rm hop}$ to dY_e/dr at $Y_e \approx 1/3$ requires special attention. In the dynamic environment of a supernova, the kth mass element is characterized by its radius $r_k(t)$, temperature $T_k(t)$, density $\rho_k(t)$, and electron fraction $Y_{e,k}(t)$ as functions of time t. The profile $Y_e(r,t)$ at a specific t is obtained from the sets $\{Y_{e,k}(t)\}$ and $\{r_k(t)\}$ formed by all mass elements. The time evolution of $Y_{e,k}(t)$ is governed by

$$\frac{dY_{e,k}}{dt} = [\lambda_{\nu_e n,k}(t) + \lambda_{e^+ n,k}(t)]Y_{n,k}(t) - [\lambda_{\bar{\nu}_e p,k}(t) + \lambda_{e^- p,k}(t)]Y_{p,k}(t), \quad (4)$$

where $Y_{n,k}(t)$ and $Y_{p,k}(t)$ are the neutron and proton fraction, respectively, and $\lambda_{\alpha\beta,k}(t)$ corresponds to the rate per target nucleon for reactions (1a) and (1b) and their reverse reactions in the mass element. For $T_k \gtrsim 10^{10}$ K, $Y_{n,k} \approx 1 - Y_{e,k}$ and $Y_{p,k} \approx Y_{e,k}$. In general, $Y_{n,k}(t)$ and $Y_{p,k}(t)$ can be followed with a nucleosynthesis network given $T_k(t)$, $\rho_k(t)$, and $Y_{e,k}(t)$, from which $\lambda_{e^+ n,k}(t)$ and $\lambda_{e^- p,k}(t)$ can also be calculated. As $\lambda_{\nu_e n,k}(t)$ and $\lambda_{\bar{\nu}_e p,k}(t)$ used to determine $Y_{e,k}(t)$ are affected by ν_e-ν_s and $\bar{\nu}_e$-$\bar{\nu}_s$ conversion, which in turn depends on $Y_e(r,t)$ obtained from the set $\{Y_{e,k}(t)\}$, we must treat this feedback in calculating $P_{\rm hop}$.

We use the data from an $8.8M_\odot$ electron-capture supernova (ECSN) simulation [53], which features the only successful explosion in spherical symmetry with a three-flavor Boltzmann neutrino transport [53,54]. In this model, an early onset of the explosion occurs at the post-bouce time $t_{\rm pb} \sim 38$ ms, which is in qualitative agreement with multidimensional simulations [55]. We take the sets $\{r_k(t)\}$, $\{T_k(t)\}$, and $\{\rho_k(t)\}$ from the simulation and increase the resolution by adding ~2,000 mass elements in the IR region so that the resonance can be resolved properly. We recalculate each $Y_{e,k}(t)$ using Eq. (4) to obtain the self-consistent $Y_e(r,t)$ in the presence of ASFC. As initial values of $Y_{e,k}(t)$, we use the Y_e profile of the simulation at $t_{\rm pb} \approx 30$ ms when the shock has already passed through the IR region. Subsequently, we use the recalculated high-resolution Y_e profile to determine which ν_e ($\bar{\nu}_e$) have crossed the IR and compute their hopping probabilities, $P_{\rm hop}(E_\nu,\mu)$. These probabilities are then combined with the distribution function of the emitted ν_e ($\bar{\nu}_e$), $f_{\nu_e(\bar{\nu}_e)}(E_\nu,\mu)$, given by the simulation to determine $\lambda_{\nu_e n,k}$ ($\lambda_{\bar{\nu}_e p,k}$) in Eq. (4).

We first consider the results for $\delta m^2 = 1.75$ eV^2 and $\sin^2 2\theta = 0.10$. We compare the original Y_e profile at $t_{\rm pb} \sim 34$ ms with the one obtained by including ASFC feedback in Fig. 1(c). ASFC results in lower Y_e values and produces a plateau at $Y_e = 1/3^+$ corresponding to $r \sim 106$ km. To understand the formation of the Y_e plateau, let us neglect for the moment ASFC and assume that the $Y_e(r)$ profile can be approximated by the equilibrium condition, $dY_e(r)/dt = 0$, which gives $Y_e(r) = Y_{\rm e,eq}(r) = [1 + (\lambda_{\bar{\nu}_e p} + \lambda_{e^- p})/(\lambda_{\nu_e n} + \lambda_{e^+ n})]^{-1}$. When ASFC is taken into account, $\lambda_{\bar{\nu}_e p}$ ($\lambda_{\nu_e n}$) is reduced to $\lambda'_{\bar{\nu}_e p}$ ($\lambda'_{\nu_e n}$) once $\bar{\nu}_e$ (ν_e) cross the IR at $Y_e = 1/3^-$ ($1/3^+$). For a region initially with $1/3^- < Y_e < 1/3^+$, $\bar{\nu}_e$ have crossed the IR but ν_e have not, so Y_e will evolve to a new equilibrium value $Y'_{\rm e,eq} > Y_e$ due to the reduction of $\lambda_{\bar{\nu}_e p}$ to $\lambda'_{\bar{\nu}_e p}$. However, if Y_e becomes larger than $1/3^+$, ν_e will have also crossed the IR. Having both $\lambda'_{\nu_e n} < \lambda_{\nu_e n}$ and $\lambda'_{\bar{\nu}_e p} < \lambda_{\bar{\nu}_e p}$ will drive Y_e below $1/3^+$ provided that $(\lambda'_{\bar{\nu}_e p} + \lambda_{e^- p}) > 2(\lambda'_{\nu_e n} + \lambda_{e^+ n})$, which is in fact fulfilled at $t_{\rm pb} \sim 100$ ms in our calculation. Based on the above discussion, for a region initially with $Y_e > 1/3^+$ and where the above condition applies, Y_e will evolve to $1/3^+$ producing a plateau limited by two radii R^- and R^+, where $Y_{e,\rm eq}(R^-) = (\lambda_{\nu_e n} + \lambda_{e^+ n})/(\lambda_{\nu_e n} + \lambda_{e^+ n} + \lambda_{\bar{\nu}_e p} + \lambda_{e^- p}) = 1/3^-$ and $Y_{e,\rm eq}(R^+) = (\lambda'_{\nu_e n} + \lambda_{e^+ n})/(\lambda'_{\nu_e n} + \lambda_{e^+ n} + \lambda'_{\bar{\nu}_e p} + \lambda_{e^- p}) = 1/3^+$. As the plateau is formed at $Y_e = 1/3^+$, where the ν_e-ν_s conversion occurs, the conversion of ν_e becomes more adiabatic than that of $\bar{\nu}_e$. Thus, a larger fraction of ν_e is converted than $\bar{\nu}_e$ due to the feedback, and hence, $E_{0.5,\nu_e} > E_{0.5,\bar{\nu}_e}$.

In Fig. 2, we show the time evolution of R_{ν_e}, shock radius $R_{\rm sh}$, $R_{\rm IR}$, and $E_{0.5}$ with and without ASFC feedback. If ASFC feedback is neglected, all ν_e and $\bar{\nu}_e$ of different E_ν have approximately the same $R_{\rm IR}$. In this case, $E_{0.5}$ and $R_{\rm IR}$ follow a similar trend: they increase due to the flattening of the Y_e profile during the initial shock expansion, and decrease later due to the steepening of the Y_e profile

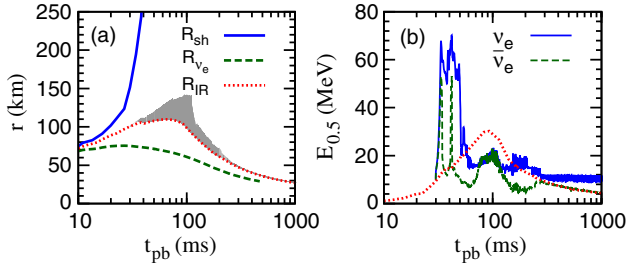

FIG. 2 (color online). (a) Evolution of R_{ν_e} (green dashed curve), $R_{\rm sh}$ (blue solid curve), and $R_{\rm IR}$ for the original (red dotted curve) and recalculated (shaded region) Y_e profiles. (b) Evolution of $E_{0.5}$ for the original (red dotted curve) and recalculated (blue solid and green dashed curves) Y_e profiles. All results for ASFC assume $\delta m^2 = 1.75$ eV^2 and $\sin^2 2\theta = 0.10$.

during the protoneutron star cooling. With the inclusion of ASFC feedback, a plateau is created at $Y_e = 1/3^+$, which becomes significantly extended in radius for $t_{\rm pb} \sim$ 32–200 ms and results in $E_{0.5,\nu_e} \gtrsim E_{0.5,\bar{\nu}_e}$. Although the detailed evolution of $E_{0.5,\nu_e(\bar{\nu}_e)}$ is associated with the dynamics and thermodynamics given by the supernova simulation, e.g., $E_{0.5,\bar{\nu}_e}$ peaks at $t_{\rm pb} \approx 42$ and 100 ms, we note that the initial fast rise of both $E_{0.5,\nu_e}$ and $E_{0.5,\bar{\nu}_e}$ to values greatly exceeding $\langle E_\nu \rangle$ during the shock expansion is a general result when ASFC operates. Because of the presence of the $Y_e = 1/3^+$ plateau, $E_{0.5,\nu_e} \geq \langle E_{\nu_e} \rangle \sim$ 10 MeV for the whole time, while $E_{0.5,\bar{\nu}_e}$ decreases at later times following the case without ASFC feedback.

As $E_{0.5,\nu_e} \gtrsim E_{0.5,\bar{\nu}_e} \gtrsim \langle E_\nu \rangle$ for most of the time, the rate of reaction (1a) is reduced more than that of reaction (1b). Also, e^- capture on protons, the inverse of reaction (1a), becomes the dominant reaction in determining the neutron richness of the ejected mass elements. Consequently, Y_e of these mass elements are greatly reduced at larger radii by ASFC compared to the case without ASFC. We show the Y_e evolution for an example mass element as a function of time in Fig. 3(a) with and without ASFC feedback. As the mass element is being ejected, it encounters the plateau of $Y_e = 1/3^+$ at $t_{\rm pb} \sim$ 90–120 ms and its Y_e is greatly reduced from the original supernova simulation values (from 0.49 to 0.37–0.39 for $t_{\rm pb} \gtrsim 200$ ms). We find that a similar reduction of Y_e by ASFC occurs in $\sim 8 \times 10^{-3}\, M_\odot$ of ejecta, which constitutes the majority of the inner ejecta.

The mass-integrated nucleosynthesis for a total inner ejecta of $\sim 10^{-2}\, M_\odot$ from this ECSN is shown in Fig. 3(b). Compared to the case without ASFC where only elements with $Z \lesssim 30$ are produced, much heavier elements from $Z = 38$ (Sr) to $Z = 48$ (Cd) are produced with ASFC and their pattern is in broad agreement with observations of the metal-poor star HD 122563 [56,57]. It remains to be explored if ASFC can help to overcome the difficulties of neutrino-driven winds from more massive supernovae in producing elements with $Z > 42$ [58]. An ECSN differs from those models by the presence of a dynamically ejected neutron-rich component [59]. This material is ejected at $t_{\rm pb} \lesssim 100$ ms and its Y_e is reduced to ~0.38 by ASFC, thereby enabling production of elements with $Z > 42$.

In view of the potential implications of ASFC for a supernova explosion, we calculate the change in the neutrino-heating rates $\dot{q}_{\nu_e n}$ and $\dot{q}_{\bar{\nu}_e p}$, which correspond to the rates of energy deposition in matter by reactions (1a) and (1b). Because of the strong ASFC of both ν_e-ν_s and $\bar{\nu}_e$-$\bar{\nu}_s$ types in the shock expansion phase, $\dot{q}_{\nu_e n}$ and $\dot{q}_{\bar{\nu}_e p}$ are reduced significantly. For the delayed neutrino-heating explosion mechanism, a crucial quantity is the net heating rate defined as the difference between the total neutrino-heating rate $\dot{q}_{\nu_e n} + \dot{q}_{\bar{\nu}_e p}$ and the total matter cooling rate $\dot{q}_{e^- p} + \dot{q}_{e^+ n}$ due to energy loss from the inverse of reactions (1a) and (1b). In Fig. 4(a) we compare the net heating rate with and without ASFC as a function of radius at $t_{\rm pb} \sim 34$ ms. It can be seen that ASFC drastically turns the region of net heating at $r \gtrsim 110$ km into one of net cooling.

While we have focused on the results for $\delta m^2 = 1.75$ eV^2 and $\sin^2 2\theta = 0.10$ so far, we have also examined the effects of ASFC on ECSN explosion and nucleosynthesis for a wide range of mixing parameters. In Fig. 4(b) we show contours of $\dot{q}'_{\nu_e n}/\dot{q}_{\nu_e n}$ and $\dot{q}'_{\bar{\nu}_e p}/\dot{q}_{\bar{\nu}_e p}$ for $r > R_{\rm IR}$ at $t_{\rm pb} \sim 34$ ms in the $(\sin^2 2\theta, \delta m^2)$ space, where $\dot{q}'_{\nu_e n}$ and $\dot{q}'_{\bar{\nu}_e p}$ are the heating rates with ASFC. The filled diamond in Fig. 4(b) represents the mixing parameters used above and the shaded regions give those inferred from reactor neutrino experiments at the 90% confidence level [14]. Except for the two regions with the lowest δm^2, all other inferred parameters for ASFC might have a large negative impact on the explosion of the $8.8 M_\odot$ ECSN, even possibly hindering the explosion. For the impact on nucleosynthesis, we show

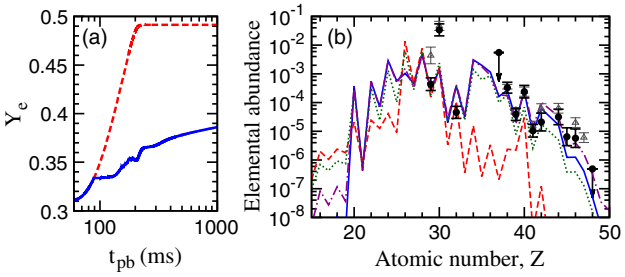

FIG. 3 (color online). Comparison of (a) Y_e evolution in an example mass element and (b) integrated nucleosynthesis with and without ASFC. Results without ASFC are shown as red dashed curves. Results with ASFC are for $(\delta m^2/\text{eV}^2, \sin^2 2\theta) = (1.75, 0.1)$ (blue solid curves), (1.0,0.06) (magenta dash-dotted curve), and (0.4,0.04) (green dotted curve). Data on the metal-poor star HD 122563 normalized to the calculated abundance of Zr ($Z = 40$) of the blue solid curve are shown as open triangles [56] and filled circles [57] in (b).

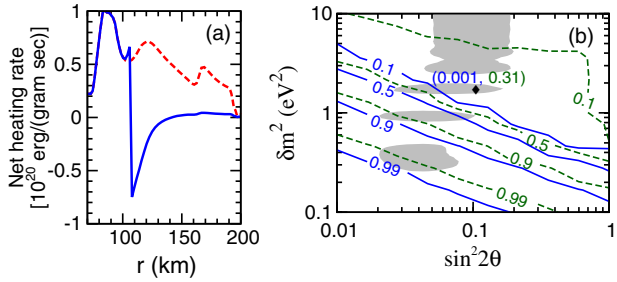

FIG. 4 (color online). (a) Comparison of the net heating rate with (blue solid curve) and without (red dashed curve) ASFC as a function of radius at $t_{\rm pb} \sim 34$ ms for $\delta m^2 = 1.75$ eV^2 and $\sin^2 2\theta = 0.10$ [filled diamond in (b)]. (b) Contours of $\dot{q}'_{\nu_e n}/\dot{q}_{\nu_e n}$ (blue solid curves) and $\dot{q}'_{\bar{\nu}_e p}/\dot{q}_{\bar{\nu}_e p}$ (green dashed curves) for $r > R_{\rm IR}$ at $t_{\rm pb} \sim 34$ ms. Numbers in parentheses give $(\dot{q}'_{\nu_e n}/\dot{q}_{\nu_e n}, \dot{q}'_{\bar{\nu}_e p}/\dot{q}_{\bar{\nu}_e p})$ for the mixing parameters used in (a). Shaded regions give mixing parameters inferred at the 90% confidence level by [14].

the integrated nucleosynthesis results corresponding to $(\delta m^2/\mathrm{eV}^2, \sin^2 2\theta) = (1.0, 0.06)$ and $(0.4, 0.04)$ in Fig. 3(b). It can be seen that the production pattern for $Z = 38$–48 does not sensitively depend on the mixing parameters. This suggests an interesting possibility that for the allowed mixing parameters with lower δm^2 and $\sin^2 2\theta$, ASFC can aid the production of the elements with $Z > 42$ but not affect strongly the explosion in an ECSN.

We have shown that the existence of sterile neutrinos with parameters inferred from reactor neutrino experiments produces substantial ASFC of the ν_e-ν_s and $\bar{\nu}_e$-$\bar{\nu}_s$ types near the core of an $8.8M_\odot$ ECSN. As a result of ASFC feedback, a Y_e plateau is formed in the resonance region where $Y_e \approx 1/3$. This further enhances conversion of ν_e into ν_s, thereby reducing Y_e at larger radii. For the inferred best-fit parameters, nuclei with $Z > 40$ are produced in a total $\sim 10^{-2} M_\odot$ of supernova ejecta with a pattern in broad agreement with metal-poor star observations. Without ASFC, only nuclei with $Z \lesssim 30$ are produced. Although ASFC can affect both the explosion and nucleosynthesis of an ECSN for a wide range of mixing parameters, we find that the neutrino-heating rates are only strongly suppressed for high values of δm^2 and/or $\sin^2 2\theta$. In contrast, the nucleosynthesis outcome is much less sensitive to the mixing parameters. Therefore, it is possible that the elements with $Z > 42$ are produced in an ECSN with the aid of ASFC but the explosion is not strongly affected.

A caveat of our treatment is that suppression of neutrino heating by ASFC would likely change the dynamic and thermodynamic conditions. Thus, the exact effects of ASFC on the supernova explosion and nucleosynthesis remain to be studied by implementing ASFC in the simulations self-consistently. These studies should also be extended to supernova models for more massive progenitors. Our results suggest that such studies can strongly constrain the mixing parameters for ASFC in combination with neutrino experiments and cosmological considerations. In the future we will examine the effects of ASFC in supernovae along with other flavor conversion processes and determine the impact on neutrino signals in terrestrial detectors. These studies along with the self-consistent treatment of neutrino flavor transformation in supernovae not only can provide unique probes of neutrino mixing, but may also help understanding a supernova explosion and the associated nucleosynthesis.

M.-R. W. is supported by the Alexander von Humboldt Foundation. T. F. acknowledges support from the Narodowe Centrum Nauki (NCN) within the "Maestro" program under Contract No. DEC-2011/02/A/ST2/00306. L. H. and G. M. P. are partly supported by the Deutsche Forschungsgemeinschaft through Contract No. SFB 634, the Helmholtz International Center for FAIR within the framework of the LOEWE program launched by the state of Hesse and the Helmholtz Association through the Nuclear Astrophysics Virtual Institute (VH-VI-417). Y.-Z. Q. is partly supported by the U.S. DOE (DE-FG02-87ER40328). We gratefully thank Hans-Thomas Janka, Irene Tamborra, and three anonymous reviewers for helpful comments and suggestions.

[1] S. Schael *et al.* (ALEPH Collaboration, DELPHI Collaboration, L3 Collaboration, OPAL Collaboration, SLD Collaboration, LEP Electroweak Working Group, SLD Electroweak Group, SLD Heavy Flavour Group), Phys. Rep. **427**, 257 (2006).
[2] J. Beringer *et al.* (Particle Data Group), Phys. Rev. D **86**, 010001 (2012).
[3] A. Aguilar-Arevalo *et al.* (LSND Collaboration), Phys. Rev. D **64**, 112007 (2001).
[4] A. Aguilar-Arevalo *et al.* (MiniBooNE Collaboration), Phys. Rev. Lett. **105**, 181801 (2010).
[5] A. Aguilar-Arevalo *et al.* (MiniBooNE Collaboration), Phys. Rev. Lett. **110**, 161801 (2013).
[6] G. Mention, M. Fechner, T. Lasserre, T. A. Mueller, D. Lhuillier, M. Cribier, and A. Letourneau, Phys. Rev. D **83**, 073006 (2011).
[7] M. A. Acero, C. Giunti, and M. Laveder, Phys. Rev. D **78**, 073009 (2008).
[8] K. Abazajian, M. Acero, S. Agarwalla, A. Aguilar-Arevalo, C. Albright *et al.*, arXiv:1204.5379.
[9] A. Hayes, J. Friar, G. Garvey, and G. Jonkmans, arXiv:1309.4146.
[10] C. Giunti, M. Laveder, Y. Li, Q. Liu, and H. Long, Phys. Rev. D **86**, 113014 (2012).
[11] M. Archidiacono, N. Fornengo, C. Giunti, S. Hannestad, and A. Melchiorri, Phys. Rev. D **87**, 125034 (2013).
[12] J. Hamann, S. Hannestad, G. G. Raffelt, I. Tamborra, and Y. Y. Wong, Phys. Rev. Lett. **105**, 181301 (2010).
[13] G. Mangano and P. D. Serpico, Phys. Lett. B **701**, 296 (2011).
[14] J. Kopp, P. A. N. Machado, M. Maltoni, and T. Schwetz, J. High Energy Phys. 05 (2013) 050.
[15] C. Giunti, M. Laveder, Y. Li, and H. Long, Phys. Rev. D **88**, 073008 (2013).
[16] A. Mirizzi, G. Mangano, N.Saviano, E. Borriello, C. Giunti, G. Miele, and O. Pisanti, Phys. Lett. B **726**, 8 (2013).
[17] L. Wolfenstein, Phys. Rev. D **17**, 2369 (1978).
[18] S. P. Mikheyev and A. Y. Smirnov, Sov. J. Nucl. Phys. **42**, 913 (1985).
[19] S. Mikheev and A. Y. Smirnov, Sov. Phys. JETP **64**, 4 (1986).
[20] M. Voloshin, Phys. Lett. A **209**, 360 (1988).
[21] K. Kainulainen, J. Maalampi, and J. Peltoniemi, Nucl. Phys. **B358**, 435 (1991).

[22] H. Nunokawa, J. Peltoniemi, A. Rossi, and J. Valle, Phys. Rev. D **56**, 1704 (1997).
[23] X. Shi and G. Sigl, Phys. Lett. B **323**, 360 (1994).
[24] S. Pastor, V. Semikoz, and J. Valle, Astropart. Phys. **3**, 87 (1995).
[25] D. O. Caldwell, G. M. Fuller, and Y.-Z. Qian, Phys. Rev. D **61**, 123005 (2000).
[26] O. Peres and A. Y. Smirnov, Nucl. Phys. **B599**, 3 (2001).
[27] J. Fetter, G. McLaughlin, A. Balantekin, and G. Fuller, Astropart. Phys. **18**, 433 (2003).
[28] J. Beun, G. McLaughlin, R. Surman, and W. Hix, Phys. Rev. D **73**, 093007 (2006).
[29] J. Hidaka and G. M. Fuller, Phys. Rev. D **74**, 125015 (2006).
[30] S. Choubey, N. Harries, and G. Ross, Phys. Rev. D **76**, 073013 (2007).
[31] J. Hidaka and G. M. Fuller, Phys. Rev. D **76**, 083516 (2007).
[32] G. M. Fuller, A. Kusenko, and K. Petraki, Phys. Lett. B **670**, 281 (2009).
[33] I. Tamborra, G. G. Raffelt, L. Hudepohl, and H.-T. Janka, J. Cosmol. Astropart. Phys. 01 (2012) 013.
[34] H. A. Bethe and J. R. Wilson, Astrophys. J. **295**, 14 (1985).
[35] B. Müller, H.-T. Janka, and A. Marek, Astrophys. J. **756**, 84 (2012).
[36] Y. Suwa, T. Takiwaki, K. Kotake, T. Fischer, M. Liebendörfer, and K. Sato, Astrophys. J. **764**, 99 (2013).
[37] S. W. Bruenn, A. Mezzacappa, W. R. Hix, E. J. Lentz, O. E. B. Messer, E. J. Lingerfelt, J. M. Blondin, E. Endeve, P. Marronetti, and K. N. Yakunin, Astrophys. J. **767**, L6 (2013).
[38] Y.-Z. Qian, G. Fuller, G. Mathews, R. Mayle, J. Wilson, and S. Woosley, Phys. Rev. Lett. **71**, 1965 (1993).
[39] Y. Qian and S. Woosley, Astrophys. J. **471**, 331 (1996).
[40] A. Arcones and F.-K. Thielemann, J. Phys. G **40**, 013201 (2013).
[41] A. Esteban-Pretel, A. Mirizzi, S. Pastor, R. Tomàs, G. Raffelt, P. Serpico, and G. Sigl, Phys. Rev. D **78**, 085012 (2008).
[42] G. Sigl and G. Raffelt, Nucl. Phys. **B406**, 423 (1993).
[43] G. M. Fuller, R. W. Mayle, J. R. Wilson, and D. N. Schramm, Astrophys. J. **322**, 795 (1987).
[44] J. T. Pantaleone, Phys. Lett. B **287**, 128 (1992).
[45] W. Hix, O. Messer, A. Mezzacappa, M. Liebendörfer, J. Sampaio, K. Langanke, D. Dean, and G. Martínez-Pinedo, Phys. Rev. Lett. **91**, 201102 (2003).
[46] K. Langanke, G. Martínez-Pinedo, J. Sampaio, D. Dean, W. Hix, O. Messer, A. Mezzacappa, M. Liebendörfer, H.-Th. Janka, and M. Rampp, Phys. Rev. Lett. **90**, 241102 (2003).
[47] G. Hinshaw *et al.* (WMAP Collaboration), Astrophys. J. Suppl. Ser. **208**, 19 (2013).
[48] P. Ade *et al.* (Planck Collaboration), arXiv:1303.5076.
[49] C. Kraus, B. Bornschein, L. Bornschein, J. Bonn, B. Flatt *et al.*, Eur. Phys. J. C **40**, 447 (2005).
[50] L. Landau, Phys. Z. Sowjetunion **2**, 46 (1932).
[51] C. Zener, Proc. R. Soc. A **137**, 696 (1932).
[52] W. Haxton, R. Hamish Robertson, and A. M. Serenelli, Annu. Rev. Astron. Astrophys. **51**, 21 (2013).
[53] T. Fischer, S. Whitehouse, A. Mezzacappa, F.-K. Thielemann, and M. Liebendorfer, Astron. Astrophys. **517**, A80 (2010).
[54] L. Hudepohl, B. Muller, H.-T. Janka, A. Marek, and G. Raffelt, Phys. Rev. Lett. **104**, 251101 (2010).
[55] H.-T. Janka, B. Mueller, F. Kitaura, and R. Buras, Astron. Astrophys. **485**, 199 (2008).
[56] S. Honda, W. Aoki, Y. Ishimaru, S. Wanajo, and S. Ryan, Astrophys. J. **643**, 1180 (2006).
[57] I. U. Roederer, J. E. Lawler, J. S. Sobeck, T. C. Beers, J. J. Cowan, A. Frebel, I. I. Ivans, H. Schatz, C. Sneden, and I. B. Thompson, Astrophys. J. Suppl. Ser. **203**, 27 (2012).
[58] G. Martnez-Pinedo, T. Fischer, and L. Huther, arXiv:1309.5477.
[59] S. Wanajo, H.-T. Janka, and B. Mueller, Astrophys. J. **726**, L15 (2011).